

Development of a time correction algorithm for a precise synchronization of a free-running Rubidium atomic clock with the GPS Time

Claire Dalmazzone,^{1a}, Mathieu Guigue,^a, Lucile Mellet,^{2a}, Boris Popov,^a,
Stefano Russo,^a, Vincent Voisin,^a,
Michel Abgrall,^b, Baptiste Chupin,^b, Caroline B. Lim,^b, Paul-Éric Pottie,^b,
Pierre Ulrich^b

^a*Laboratoire de Physique Nucléaire et des Hautes Energies (LPNHE), Sorbonne
Université, CNRS/IN2P3, 4 place Jussieu, Paris, 75005, France*

^b*LNE-SYRTE, Observatoire de Paris, Université PSL, CNRS, Sorbonne Université, 61
avenue de l'Observatoire, Paris, 75014, France*

Abstract

We present results of our study devoted to the development of a time correction algorithm needed to precisely synchronize a free-running Rubidium atomic clock with the Coordinated Universal Time (UTC). This R&D is performed in view of the Hyper-Kamiokande (HK) experiment currently under construction in Japan, which requires a synchronization with UTC and between its different experimental sites with a precision better than 100 ns. We use a Global Navigation Satellite System (GNSS) receiver to compare a PPS and a 10 MHz signal, generated by a free-running Rubidium clock, to the Global Positioning System (GPS) Time signal. We use these comparisons to correct the time series (time stamps) provided by the Rubidium clock signal. We fit the difference between Rubidium and GPS Time with polynomial functions of time over a certain integration time window to extract a correction of the Rubidium time stamps in offline or online mode. In online mode, the latest fit results are used for the correction until a new comparison to the GPS Time becomes available. We show that with an integration time window of around 10^4 seconds, we can correct the time stamps drift caused

¹Corresponding author: claire.dalmazzone@lpnhe.in2p3.fr, +33617925827

²Now at Michigan State University, Department of Physics and Astronomy, East Lansing, Michigan, USA

by the frequency random walk noise and the deterministic frequency drift of the free running Rubidium clock so that the time difference with respect to the GPS Time stays within a ± 5 ns range in both offline or online correction mode.

Keywords: timing detectors, precise timing, atomic clock, GPS, UTC

PACS: 06.30. -k, 06.30.Ft, 07.05.Fb

2000 MSC: 00A79, 85-05, 85-08

1. Introduction

A precise synchronization with the Coordinated Universal Time (UTC) or with another signal is a necessity in many applications, particularly in long-baseline physics experiments including several experimental sites. A good example is long-baseline neutrino oscillation experiments, like OPERA [1] (2006-2012), T2K [2] (from 2010) and NOvA [3] (from 2014), where a beam of neutrinos is produced and characterized in a first experimental site and detected, after several hundreds of kilometers of propagation, at another site to measure a change of the beam properties. Two next generation long-baseline neutrino experiments are being built at the moment: Hyper-Kamiokande (HK) [4] that plans to start taking data in 2027 and DUNE [5][6] that should begin sometime after 2029. These experiments require a synchronization of 100 ns or better between the different experimental sites. Moreover, multi-messenger programs that plan to compare different components of astrophysical events [7] (e.g.: gamma-ray bursts, gravitational waves, neutrino emissions of supernovae, etc.) require a synchronization with UTC of different experiments located all over the world. For instance, to enter the SuperNova Early Warning System (SNEWS) network [8], a synchronization to UTC better than 100 ns is required.

Many long-baseline physics experiments use atomic oscillators as frequency references because of their good short term stability. Among the reference oscillators available on the market, Rubidium atomic clocks are generally chosen for their affordability as it was the case for the T2K [9] and Super-Kamiokande [10] timing systems. However, Rubidium clocks usually drift away from a stable reference because of frequency drift and random walk. For synchronization to UTC, this drift usually needs to be prevented or corrected. A common solution is to discipline the average frequency of the clock to the signals of an external Global Navigation Satellite System

29 (GNSS) receiver, with an integration time window chosen so that it does not
30 deteriorate the short term stability of the clock. However, it presents some
31 drawbacks like the fact that the user has little control on the setup. In case
32 of problems (like jumps in the time comparison), it is difficult to understand
33 where they come from (GPS Time, receiver, the master clock, etc.) and
34 to assess the uncertainty on the synchronization to UTC. The R&D work
35 presented in this paper and introduced in [11] is focused on designing and
36 characterizing an alternative method that allows more freedom to the user
37 and a better understanding of the process. It is based on known metrology
38 techniques [12, 13]. The proposed method uses a free-running atomic clock
39 to derive a time signal and provide time stamps. In a physics experiment
40 these would be the time stamps of detected events. The time stamps are
41 corrected in post-processing using comparisons of the Rubidium clock signal
42 to GNSS Time. In that way, we can store all the information (the raw signal,
43 the comparisons to GPS Time, the derived correction etc.) and apply the
44 correction in either online (during the data-acquisition) or offline modes. Let
45 us note that the GNSS time is a good approximation of the UTC, within a
46 few nanoseconds, and it allows synchronization to UTC via a common-view
47 technique [14]. The common-view would be performed with a national labo-
48 ratory providing a local realization of UTC(k), like e.g. the NICT laboratory
49 in Japan [15], then the conversion to UTC can be performed with the help of
50 the Circular T of the BIPM (Bureau International des Poids et Mesures) [16]
51 at the end of each month.

52 **2. Materials and Methods**

53 *2.1. Experimental setup*

54 The experimental setup that we used is schematized in Figure 1. It is
55 located at the Pierre and Marie Curie (Jussieu) campus of the Sorbonne
56 University in Paris. The setup consists of two main parts: one represents
57 the timing generation and correction setup, that could be reproduced in the
58 HK experiment, and the second part is related to testing the efficiency of the
59 correction method. In the first part a Rubidium clock (Rb) in free-running
60 mode, at the ground floor of the laboratory, generates a Pulse Per Second
61 (PPS) signal and a 10 MHz signal that are transported to the fifth floor
62 with the White Rabbit (WR) protocol. The timing signals of the slave WR
63 switch are used by a GNSS receiver as a reference for its internal clock. The
64 receiver connected to its antenna on the roof, above the fifth floor, is used to

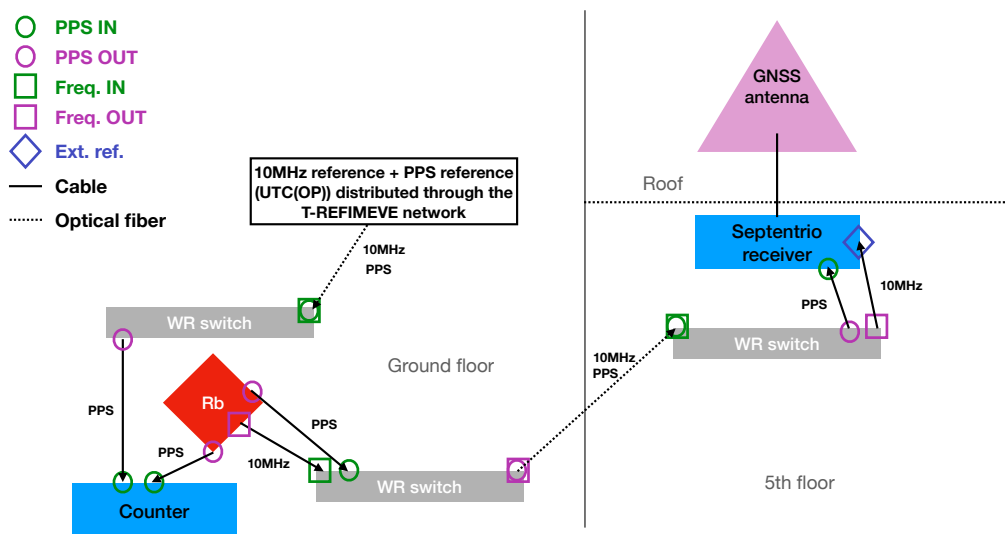


Figure 1: Experimental setup used in this work. Part of the equipment is installed at the ground floor and the other part at the fifth floor. The relevant signals generated at the ground floor are transported to the fifth floor via optical fibers with the White Rabbit (WR) protocol. This particular setup mimics what could happen in underground experiments where the clock signal would be generated underground whereas the GNSS antenna and receiver would be located above-ground.

65 measure time comparisons between the GPS Time and the Rubidium clock.
 66 This physical distance between the time generation part and the receiver was
 67 done on purpose to mimic what would happen in many long-baseline physics
 68 experiments. Indeed, in Hyper-Kamiokande, the Rubidium clock would be
 69 placed inside a mountain, where a cavern has been dug to host the detector,
 70 whereas the receiver would have to be placed outside in a valley. The second
 71 part of our experimental setup is contained in the experimental room at the
 72 ground floor and its purpose is to validate the performance of the method
 73 and would thus not be reproduced in the final setup in Hyper-Kamiokande.
 74 It consists of a counter measuring the time difference between the Rubidium
 75 clock PPS signal and the French realization of UTC (called UTC(OP) for
 76 Observatoire de Paris). The UTC(OP), as well as a 10 MHz reference signal,
 77 are available at the laboratory, as part of the T-REFIMEVE network, via a
 78 third White Rabbit switch.

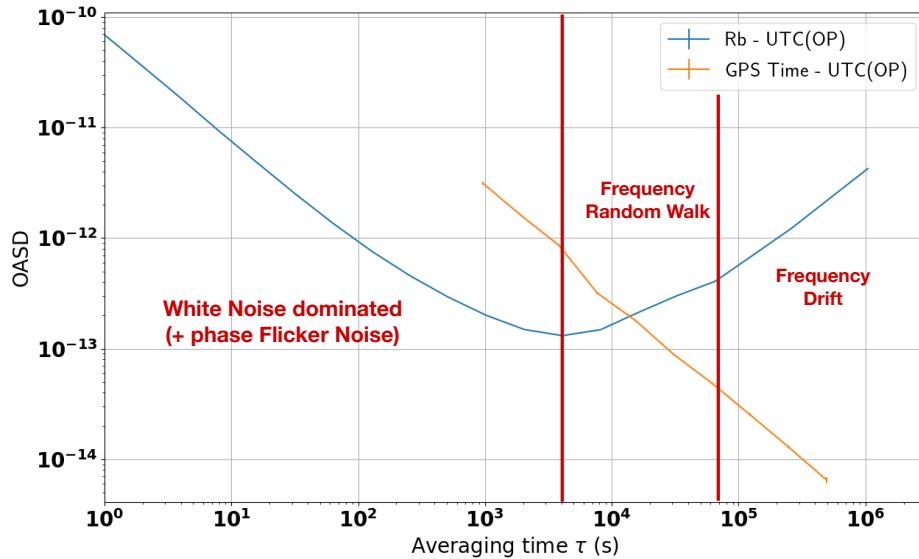


Figure 2: Overlapping Allan Standard Deviation of the Rb vs UTC(OP) time difference (in blue), measured by the counter, before any correction, and of GPS Time vs UTC(OP) (in orange) measured by the Septentrio receiver. The main types of noises affecting the Rubidium clock stability are indicated where they are limiting the stability.

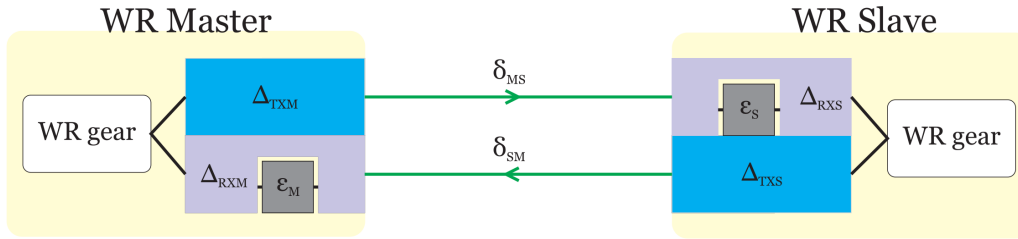


Figure 3: White Rabbit link model, from [19]

79 *2.1.1. Rubidium clock*

80 The Rubidium atomic clock used is the FS725 Rubidium Frequency Stan-
 81 dard sold by Stanford Research Systems integrating a rubidium oscillator of
 82 the PRS10 model. It provides two 10 MHz and one 5 MHz signals with low
 83 phase white noise and its stability estimated via the Allan Standard Devi-
 84 ation (ASD) [17] at 1 s is about 2×10^{-11} . It also provides a PPS output
 85 with a jitter of less than 1 ns. Its 20 years aging was estimated to less than
 86 5×10^{-9} and the Mean Time Before Failure is over 200,000 hours. It can also
 87 be frequency disciplined using an external 1 PPS reference, based on GPS
 88 for instance. The FS725 is installed at the ground floor of our laboratory
 89 and its 10 MHz and 1 PPS output are transported to the GNSS receiver at
 90 the fifth floor.

91 *2.1.2. White Rabbit switches*

92 The White Rabbit (WR) project [18] is a collaborative effort involving
 93 CERN, the GSI Helmholtz Centre for Heavy Ion Research, and other part-
 94 ners from academia and industry. Its primary objective is to develop a highly
 95 deterministic Ethernet-based network capable of achieving sub-nanosecond
 96 accuracy in time transfer. Initially, this network was implemented for dis-
 97 tributing timing signals for control and data acquisition purposes at CERN's
 98 accelerator sites. The described experimental setup uses two WR switches
 99 to propagate with great precision the Rubidium clock PPS and frequency
 100 signals from the ground floor to the fifth floor.

101 The calibration of the link allows to obtain a sub-nanosecond synchrono-
 102 zation between switches. A White Rabbit link between two devices is char-
 103 acterized by specific hardware delays and fiber propagation latencies. Each
 104 WR Master and WR Slave possesses fixed transmission and reception delays
 105 (ΔT_{XM} , ΔRXM , ΔT_{XS} , ΔRXS). These delays are the cumulative result

106 of various factors such as SFP transceiver, PCB trace, electronic component
107 delays, and internal FPGA chip delays. Additionally, there is a reception
108 delay on both ends caused by aligning the recovered clock signal to the inter-
109 symbol boundaries of the data stream, referred to as the bitslide value (ϵ_M
110 and ϵ_S in Figure 3). We can see the results of calibration process using a
111 counter in Figure 4, the difference of PPS signals between the WR slave and
112 master switches changes from 165 ps to 60 ps (with a 100 m long fiber).
113 Delays introduced by the cables were subtracted to the mean values.

114 As a part of the T-REFIMEVE network [20, 21], the LPNHE has ac-
115 cess through a dedicated switch to the official French realization of the
116 UTC, called UTC(OP) (for Observatoire de Paris) [22], transported from
117 the SYRTE laboratory via White Rabbit protocol. REFIMEVE is a French
118 national research infrastructure aiming at the dissemination of highly ac-
119 curate and stable time and frequency references to more than 30 research
120 laboratories and research infrastructures all over France. The reference sig-
121 nals originate from LNE-SYRTE and are mainly transported over the optical
122 fiber backbone of RENATER, the French National Research and Education
123 Network. The UTC(OP) signal was not used in the final experimental setup
124 because we do not foresee to have access to such a high precision signal in
125 HK experiment. It was however used to characterize the GPS Time signal
126 measured by the Septentrio receiver and whose OASD is shown in Figure 2.

127 *2.1.3. Counter*

128 The counter is the 53220A model from Keysight Technologies. here it
129 was used to measure the time interval between the two PPS signals: the
130 UTC(OP) PPS reference and the one generated by the free-running Rubid-
131 ium. The input channel(s) are (default) configured for auto-leveling at 50%
132 with a positive slope.

133 *2.1.4. Septentrio GPS antenna and receiver*

134 We use the Septentrio PolaNt Choke ring GNSS antenna that supports
135 GNSS signals from many satellite constellations including GPS, GLONASS,
136 Galileo and BeiDou. In this work, we restrict the analysis to GPS but it can
137 easily be generalized to any subset of constellations. The antenna position
138 has been previously measured to a precision better than 6 mm by trilateration
139 with the help of a web-based service provided by Canadian government [23].
140 We use a Septentrio PolARx5 GNSS reference receiver as a timing receiver to
141 compare GPS Time to the Rubidium clock. The receiver performs measure-

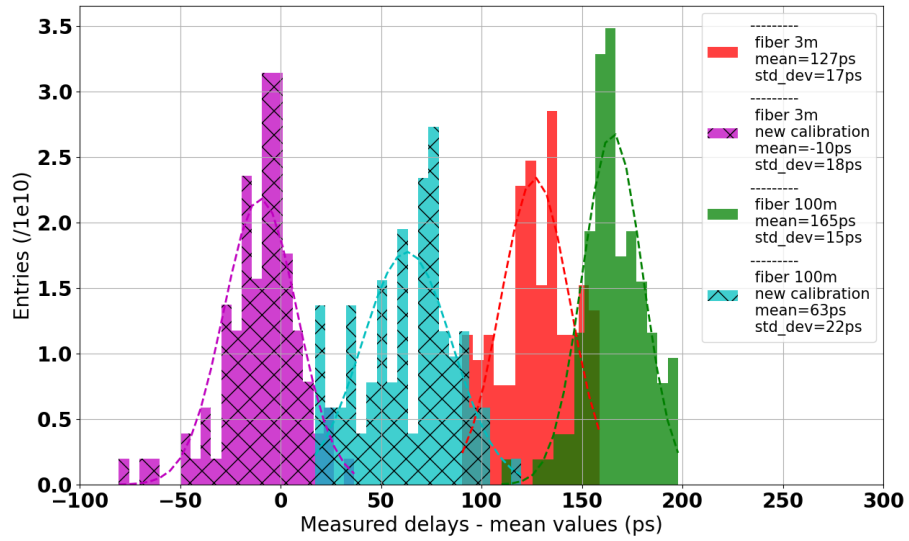
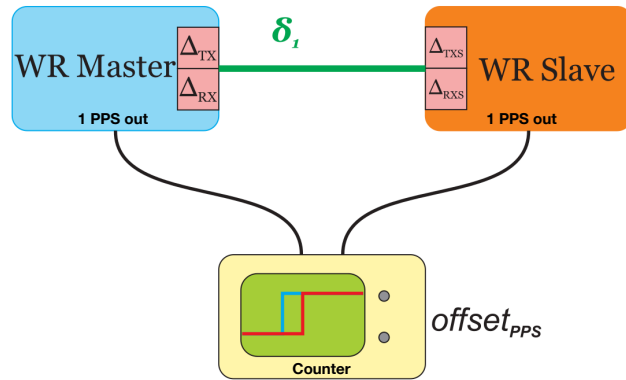


Figure 4: Difference between the PPS OUT signals of the White Rabbit slave and master switches before and after calibration

142 ments based on the 10 MHz reference signal coming via White Rabbit from
 143 the Rubidium clock. The Rubidium clock 1 PPS signal is also transported
 144 to the receiver via White Rabbit to allow, at initialization, to identify the
 145 10 MHz cycle. Note that this 1 PPS input is kept during the whole data-
 146 taking to avoid possible phase jumps due to perturbations. The Septentrio
 147 receiver provides one measurement every 16 min which is the middle point of
 148 the linear function fitted from the 13 min of data from the beginning of this
 149 16 min time window. The results of the measurements are registered using
 150 the CGGTTS file format [24].

151 Before taking measurements, the whole system has been calibrated against
 152 official reference signals from the SYRTE laboratory. As it can be seen in
 153 Figure 5, the following delays need to be measured and taken into account
 154 during operation [25]. The calibration procedure [26] consists in measuring
 155 these:

- 156 • X_S : internal delay inside the antenna, frequency dependent
- 157 • X_C : delay caused by the antenna cable
- 158 • X_R : internal delay of the receiver for the antenna signal, frequency
 159 dependent
- 160 • X_P : in case an external signal is given in input, connection cable delay
- 161 • X_O : in case an external signal is given in input, internal receiver delay
 162 between external 1 PPS and internal clock

163 X_S and X_R depend on the GNSS carrier frequency that is being tracked,
 164 meaning it is specific to each frequency of each GNSS constellation. The cal-
 165 ibration was performed for both GPS and Galileo constellations, each having
 166 two available carrier frequencies. The cable delays X_C and X_P were evaluated
 167 with an oscilloscope by sending a pulse in the cable and measuring the timing
 168 of the reflection. To reproduce the experimental conditions of underground
 169 experiments like HK or DUNE where the GPS antenna is outside, away from
 170 the detector, a 100 m cable was used and calibrated. The total cable delay
 171 was measured to be 505 ns. The internal delays of the antenna and receiver
 172 can only be measured together (for each frequency) as $INTDLY = X_S + X_R$.
 173 This was done through a comparison with OP73, one of the calibrated GNSS
 174 stations of SYRTE, and with UTC(OP), the French realization of UTC, as
 175 an input to the two receivers. The values of INTDLY found for the two most

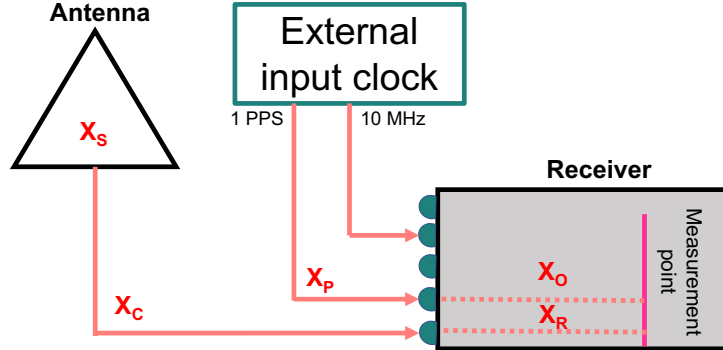


Figure 5: Delays to consider for the selected GNSS receiver+antenna pair, from [27]

176 widely available carrier frequencies of the GPS constellation (L1 and L2) and
 177 the Galileo constellation (E1 and E5a) are given in Table 1.

Table 1: Values of INTDLY in ns found for the first antenna+receiver system calibrated at the SYRTE laboratory against the OP73 station

GPS L1	GPS L2	Galileo E1	Galileo E5a
25.832	22.871	28.242	25.431

178

179 The delays X_C , INTDLY, and REFDLY can then be given as parameters
 180 of the receiver so that they are automatically handled in any further use of
 181 the receiver. Uncertainties on the measured delays were evaluated to 4 ns ac-
 182 cording to estimations fixed for the employed method. The calibration needs
 183 to be re-done for any new antenna+receiver+antenna cable combination.

184 2.2. Corrections methods

185 2.2.1. General principle

186 To synchronize the Rubidium time stamps to UTC, we apply a time-
 187 dependent correction (quadratic or linear) to the time series generated by
 188 the free-running Rubidium clock $\phi_{Rb}(t)$. We model the k^{th} portion of the
 189 time series ($dt_{Rb,GPS}$), defined as the difference between the free-running Rb
 190 clock and the GPS Time, as a (one or two degrees) polynomial of time

$$\forall t \in [t_{k-1}, t_k], dt_{Rb,GPS}(t) = a_k \cdot t^2 + b_k \cdot t + c_k. \quad (1)$$

191 The coefficients a_k ($a_k = 0$ in case of linear fit), b_k and c_k of the polynomials
 192 are extracted from least square polynomial fits of the time difference distri-
 193 butions. The fits of these differences, obtained from the Septentrio receiver,
 194 are performed for every k^{th} time window of length Δt . In other words, we
 195 model the Septentrio measurements with a piece-wise polynomial function of
 196 time. For the k^{th} time window (between t_k and t_{k+1}), we get the corrected
 197 time stamps

$$\forall t \in [t_k, t_{k+1}], \phi_{Rb,corr}(t) = \phi_{Rb}(t) - a_k \times t^2 - b_k \times t - c_k. \quad (2)$$

198 The time-length Δt of the pieces (time windows) has to be chosen carefully.
 199 In particular, it should be short enough in order to correct for the effect of
 200 the frequency random walk of the Rubidium clock.

201 In the following, we consider two types of correction: the offline and the
 202 online corrections. The difference between the two methods is illustrated in
 203 Figure 6. The offline correction consists in using the Septentrio data from
 204 the same time-window as the Rubidium signal to extract the a_k , b_k and c_k
 205 coefficients. This correction is called offline because it requires the Septentrio
 206 data from up to $t_k + \Delta t = t_{k+1}$ to correct all the time stamps between t_k and
 207 t_{k+1} so it cannot be performed in real-time (one would need to wait a time
 208 Δt to extract the correction coefficients for the t_k time stamp).

209 The online correction consists in correcting the Rubidium time stamps
 210 between t_k and t_{k+1} using Septentrio data collected before t_k . One example
 211 of online correction is illustrated in Figure 6 where overlapping windows are
 212 used. This method is called online because it can be applied in real time.
 213 In the following, we will consider the most frequent possible update of the
 214 a_k , b_k and c_k coefficients: they will be updated every time we receive a new
 215 data point from the Septentrio receiver (every $\delta t \approx 16$ minutes in our case).
 216 This means that we have $t_{k+1} = t_k + \delta t$ so that the a_k , b_k and c_k coefficients
 217 are extracted using Septentrio data between $t_k - \Delta t$ and t_k and are used
 218 to correct the time stamps between t_k and $t_k + \delta t$. In that particular case
 219 every Septentrio data point will have been used in multiple fits, the number
 220 depending on the length of the fit time window Δt .

221 The performance of the correction is evaluated in two ways. First, we look
 222 at the stability of the corrected time series estimated with the Overlapping
 223 Allan Standard Deviation (OASD). Then, we also look at the time difference
 224 against GPS signal after correction.

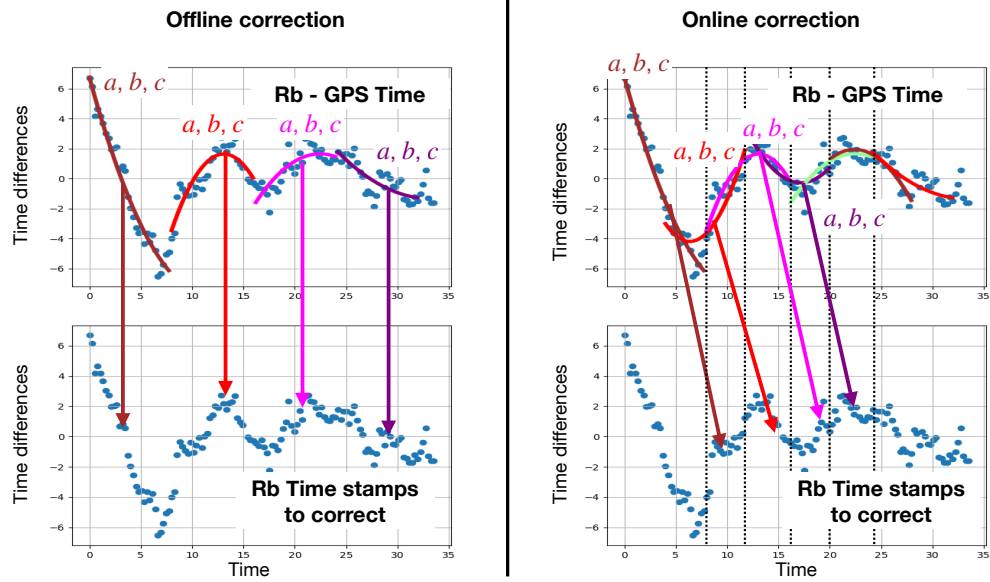


Figure 6: Schematic representation of the offline (left) and online (right) corrections. In the offline correction, we extract the correction coefficients using Rubidium - GPS Time comparison from the same time-window as the data we want to correct. In the online correction, we use Rubidium - GPS Time comparison from the previous time-window with respect to the data interval we want to correct. Only the second correction can be applied in real time as it only requires comparisons with GPS Time from previous measurements.

225 *2.2.2. Validation of the method with simulations*

226 Before evaluating the performance of our timing system when integrating
 227 the correction algorithm, the method was validated on simulated signals [27]
 228 in order to isolate the effect and performance of the correction from any
 229 measurement effect.

230 ***Simulation details.*** Three types of signals were considered: a perfect clock
 231 to be used as a reference to evaluate the performance, a free-running Rubid-
 232 ium clock and a GPS time signal, as measured by the Septentrio receiver.
 233 The quadratic drift was not included because it is deterministic and therefore
 234 does not require further study for being corrected. At first order, the clock
 235 signal can be modeled by white noise (WN) in both phase and frequency as
 236 well as a random walk (RW) noise in frequency. Based on the characteriza-
 237 tion of the Rb clock, the phase and frequency flicker noises can be neglected
 238 for this purpose. Indeed, the characterization of our Rubidium clock in Fig-
 239 ure 2 showed that the frequency flicker noise had a negligible impact on the
 240 OASD. Furthermore, the phase white and flicker noises have a similar impact
 241 on the standard OASD and cannot be distinguished here. We chose to ignore
 242 the phase flicker noise as it is less straightforward to simulate and it should
 243 not impact the long term random walk that we want to correct. The GPS
 244 Time can be modeled as pure phase white noise. The corresponding OASD
 245 as a function of the averaging time τ can be modeled [28, 29, 30] by:

$$OASD(\tau) \cong A_{WNp} \times \tau^{-1} + A_{WNf} \times \tau^{-1/2} + A_{RWf} \times \tau^{+1/2}. \quad (3)$$

246 The amplitudes A of these main frequency and phase noises were determined
 247 through fitting this model (Eq. 3) to the OASD of the data when character-
 248 izing our equipment (see Figure 2) and found to be:

$$\begin{aligned} A_{WNf} &= 7 \times 10^{-12} \text{ s}^{1/2}, \\ A_{RWf} &= 1 \times 10^{-15} \text{ s}^{-1/2}, \\ A_{WNp} &= 5 \times 10^{-11} \text{ s}, \end{aligned} \quad (4)$$

249 for the free-running Rb clock and for the GPS Time:

$$\begin{aligned} A_{WNf} &= 0 \text{ s}^{1/2}, \\ A_{RWf} &= 0 \text{ s}^{-1/2}, \\ A_{WNp} &= 2 \times 10^{-9} \text{ s}, \end{aligned} \quad (5)$$

250 with indices f and p for frequency and phase respectively. Using random
 251 numbers generation and a model with these types of noise discussed just
 252 above, time series were simulated.

253 The equivalent of 10^6 s of data was simulated. To mimic the output of
 254 the GNSS receiver, time differences between the simulated Rubidium clock
 255 and the simulated GPS Time (Δt_{Rb-ref}^i) are computed every 16 mn.

256 **Offline corrections.** First, the offline corrections were tested on the sim-
 ulated data. In Figure 7, the uncorrected simulated signals of the GPS and

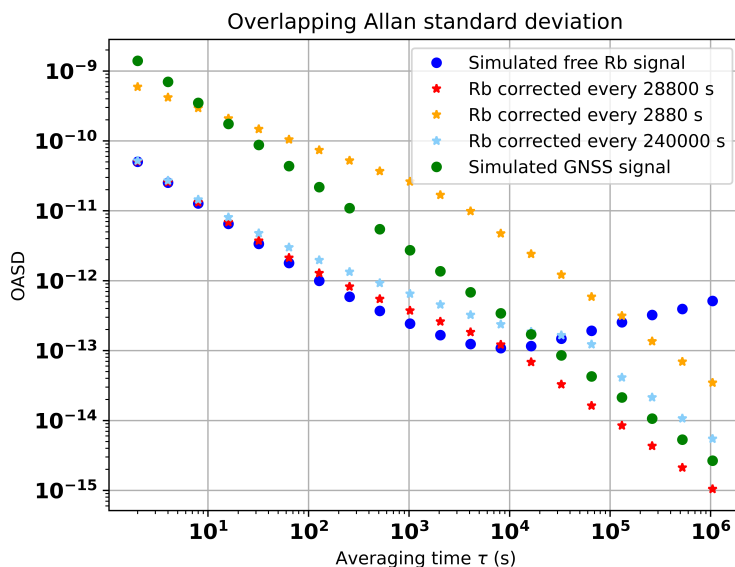


Figure 7: Comparison of overlapping ASD for corrected signals, with offline correction, with different time windows

257 the clock are reported in dotted symbols for comparison. The increase of
 258 the clock's OASD after $\tau = 10^4$ s due to the random walk is clearly visible.
 259 One can see that the OASD of the corrected signals (starred symbols) do
 260 eliminate the random walk at longer terms which indicates a success of the
 261 correction method (quadratic). Moreover, one can determine that the ideal
 262 length Δt of the correction time windows lies around 3×10^4 s which cor-
 263 responds logically to the intersection of the free-running Rb clock and GPS
 264 Time OASD curves. Indeed, the red curve with a time window of 28800 s
 265 shows an ideal combination of the short-term stability of the clock and the
 266

267 absence of random walk at longer scales. On the opposite, the yellow (shorter
 268 time window) and light blue (longer time window) curves show respectively
 269 a degradation of the short term performance and a remaining random walk
 270 component in the region between $\tau = 10^4$ s and the time window length (here
 271 240000 s).

272 **Online corrections.** The online (linear) correction method was then ap-
 273 plied to the simulated data using time series directly and a correction win-
 274 dow length of $\Delta t = 3 \times 10^4$ s. The results are shown in Figure 8 in red and
 275 prove to be just as efficient as the offline correction method to remove the
 276 random walk at longer time scales which is the main goal. The overall preci-
 277 sion on the long term region (after $\approx 10^3$ s) is as expected slightly degraded
 278 compared to the offline correction.

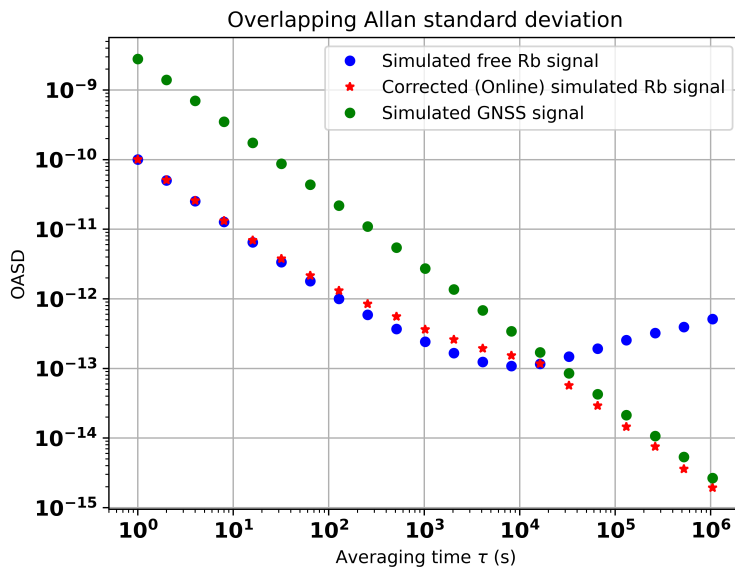


Figure 8: After online corrections at 3×10^4 s: Overlapping ASD with respect to perfect signal

279 **Conclusion on simulation.** As a conclusion, it can be said that the ap-
 280 plication of the correction algorithms to the simulated signals allowed us to
 281 validate the chosen correction methods, both the offline and online ones. In-
 282 deed, looking at the residuals after correction in Figure 9, one can see that

283 the remaining variations for both methods are well within the experimen-
 284 tal requirements as they stay within a few ns. Seven different simulations
 285 were produced to take into account statistical fluctuations and the remaining
 286 time variations were found to be for offline and online corrections respectively
 287 $\sigma_{Off} = 0.64 \pm 0.06$ ns and $\sigma_{On} = 1.15 \pm 0.07$ ns.
 288 Finally, it is important to note that although this validates the methods for
 289 application on data, those are simplified simulations, in particular because
 290 only the main noise types are taken into account. As a result, we do expect
 291 differences of performance of the correction on real data. It is also possible
 292 that the optimal time window for the correction is slightly different for real
 293 data because the simulations are not exact representation of data. Two main
 294 differences can be noted: the absence of frequency drift and flicker noises in
 295 the simulated Rubidium signal and the fact that we assume a perfect signal
 296 to compare the Rubidium signal to when evaluating the OASD.

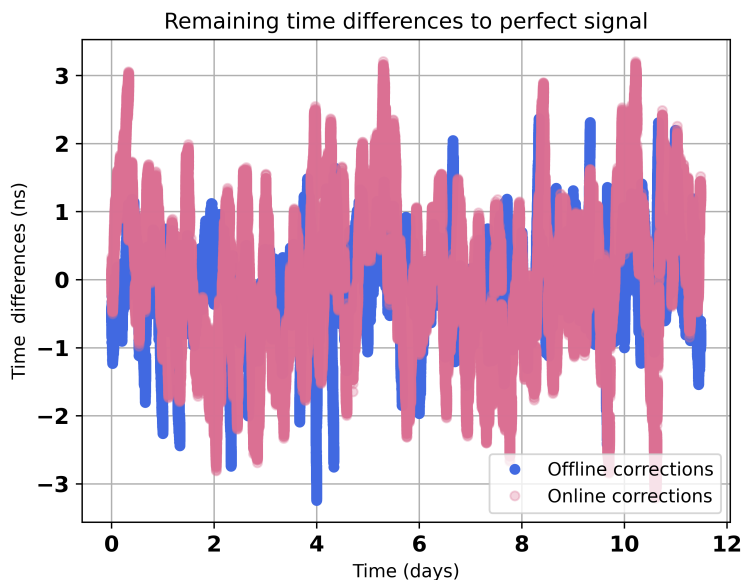


Figure 9: Comparison of time variations for simulated signals corrected with the offline method (blue) or with the sliding interval online method (pink)

297 2.2.3. Implementation on data

298 To check the impact of the correction we compare the Rubidium clock
 299 signal to the UTC(OP) that we receive at the laboratory via the Refimeve

300 network. The UTC(OP) time signal plays the role of the perfect signal used
 301 for the simulations, while obviously not being perfect. This first difference
 302 is to take into account while comparing performances on simulated data to
 303 performance on experimental data. In the following, we will also quantify the
 304 stability of the Rubidium signal using the OASD of a time series (according to
 305 equation (10) of [31]) consisting of time differences between this signal and
 306 the UTC(OP). Measuring this time difference frequently, once per second
 307 for instance, would allow to also evaluate the very short term stability of
 308 the corrected signal which is not possible with the Septentrio measurements
 309 that are integrated over 16 minutes. We use the counter to provide such a
 310 measurement every 1 second approximately. We then perform a simultaneous
 311 correction of the Rubidium - GPS Time, as measured by the Septentrio
 312 receiver, and of this measured time series. Comparing the OASD of the
 313 corrected time series to the uncorrected one, one can quantify the short
 314 term stability (below 16 minutes) after correction while making sure that the
 315 random walk was corrected. We can also use this comparison to optimize the
 316 value of Δt in order to achieve the lowest Allan Standard Deviation possible
 317 at all averaging time windows.

318 **3. Results**

319 In this Section, we present the results of the correction of the Rubidium
 320 clock time stamps obtained for simultaneous measurements of ~ 35 days
 321 with the Septentrio receiver and the counter. The OASD of the time series
 322 measured by the counter is shown in Figure 2. Note that the statistical
 323 uncertainty on the estimated OASD, due to the limited number of samples
 324 per averaging time, are included as error bars for both curves (Rb and GPS)
 325 but they are too small to be visible. Indeed for the Rb vs UTC(OP) OASD,
 326 the statistical uncertainty is at the permil level. Up to an averaging time
 327 of around $4 \cdot 10^3$ s, the stability is limited only by the phase white noise
 328 and then by the frequency white noise. After that, the OASD first increases
 329 as $\tau^{1/2}$ which is characteristic of the frequency random walk. From $\tau \approx$
 330 7×10^4 s, the OASD increases proportionally to τ . This is characteristic of a
 331 deterministic frequency drift which can be easily characterized and corrected
 332 for contrary to the frequency random walk. In comparison, the OASD of the
 333 difference between GPS Time and UTC(OP) that we receive from the SYRTE
 334 laboratory via White Rabbit network, is only limited by a phase white noise
 335 at least up to an averaging time of 5×10^5 s: the OASD keeps decreasing with

336 the averaging time. At low averaging times, the GPS stability is worse than
 337 that of the Rb because of this phase white noise: the GPS OASD is of around
 338 3×10^{-12} at 960 s compared to around 2×10^{-13} OASD for the Rubidium
 339 clock. However, at around 10^4 s, the stability of the Rb signal becomes worse
 340 compared to GPS Time because of the frequency random walk and drift of
 341 the Rubidium clock.

342 In this paper, we used only the GPS satellites with an elevation angle (an-
 343 gle between line of sight and horizontal direction) larger than 15° to extract
 344 the Rubidium time residuals distribution. During the whole data-taking pe-
 345 riod, for each data point, the Septentrio receiver was able to track an average
 346 of 6.5 GPS satellites and at least 4 GPS satellites for each data point. To
 347 obtain the Rubidium vs GPS Time difference, we take the mean value of the
 348 differences between the Rubidium clock and each GPS satellite tracked in
 349 the same integration time window of the Septentrio receiver. The obtained
 350 time difference is shown in Figure 10. It shows that the Rubidium clock time
 351 signal drifts away from the PS Time in a quadratic function of time because
 352 of the frequency linear drift. After around 35 days, the difference surpasses
 353 $25 \mu\text{s}$. A zoom on the first five days of data also shows some shorter term
 354 fluctuations characteristic of the frequency random walk. Because of those
 355 two sources of frequency drift, we see that after a few days of data-taking,
 356 the Rubidium clock time signal can drift away from the GPS Time by more
 357 than a hundred nanoseconds.

358 3.1. Offline correction

359 Figure 11 shows the Allan Standard Deviation of the Rubidium-UTC(OP)
 360 data. Note that the measurement rate of the counter was of around 0.995
 361 measurement per second. The blue curve shows the result for the raw series,
 362 before any correction. The other colored curves show the results for the
 363 series corrected offline, with different width of the correction time window.
 364 Here, we use quadratic fits of the Septentrio data (so $a_k \neq 0$ a priori). The
 365 shortest time window (2880 s) corresponds to approximately 3 Septentrio 16
 366 minutes epochs. The medium (10560 s) and largest (240,000 s) correspond
 367 respectively to 11 and 250 Septentrio data points.

368 One sees that with the medium time window compared to the two oth-
 369 ers, we obtain the best stability at all averaging times. At lower averaging
 370 times, the performance is very similar to the uncorrected time series. At
 371 higher averaging times, the Allan Standard Deviation is much better than
 372 the uncorrected series as it keeps decreasing with increasing τ . This is also

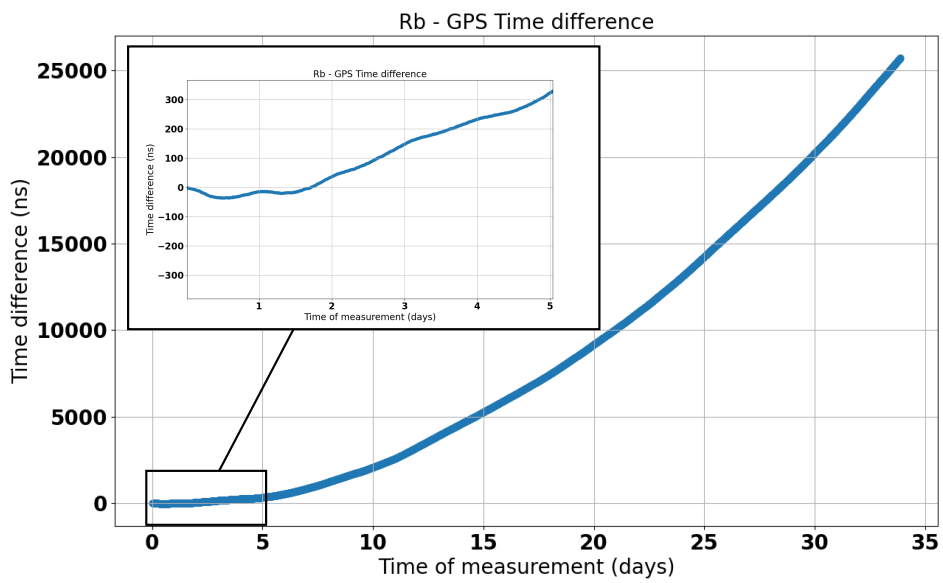


Figure 10: Time difference between the Rubidium clock and GPS Time as measured by the Septentrio receiver. The long term quadratic drift is due to the linear frequency drift of the clock. The zoom on the first five days of data also shows shorter term fluctuations caused by the frequency random walk of the Rubidium clock.

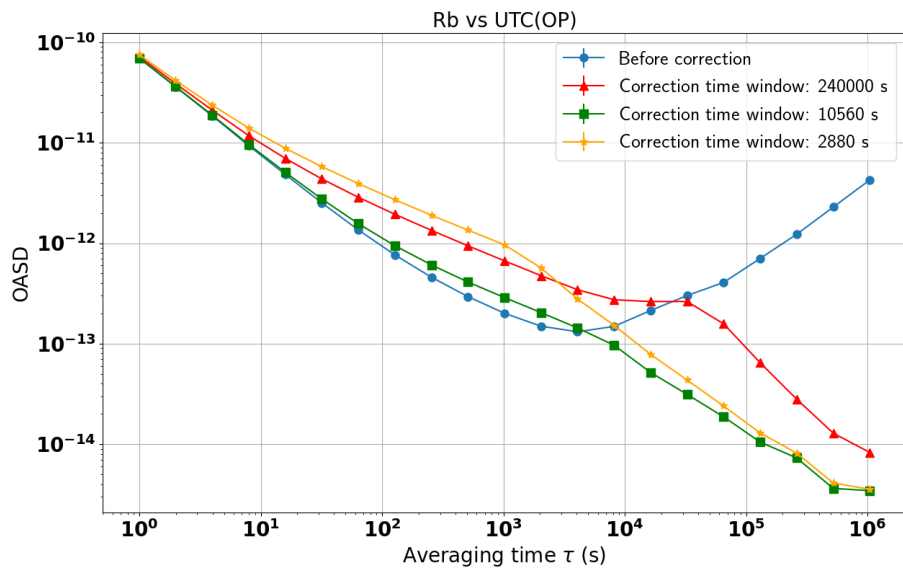


Figure 11: Overlapping Allan Standard Deviation of the Rb/PHM frequency ratios series after the deterministic drift correction (in blue) and after the correction with a correction time window of 2880 s (orange), 10560 s (green) and 240,000 s (red). The best stability at both short and long averaging times is obtained for the medium time window (10560 \approx 3 hours).

373 the case for correction with the shortest time window. This illustrates the
374 fact that both the 2880 s and 10560 s windows are able to correct very well
375 the frequency random walk and linear drift of the uncorrected time series.
376 However, with the shortest correction time window, the short term stability
377 of the time series is degraded compared to the uncorrected series: the value
378 of the ASD at 100 s increases by a factor ~ 3 . In this scenario, the corrected
379 Rubidium time signal gets very close to GPS Time which is known to have a
380 higher phase White Noise. Finally, the longest correction time window leads
381 to a similar stability as the shortest one for a small τ , and poorer stability
382 at large τ (above $5 \cdot 10^3$ s).

383 Figure 12 shows the Rubidium vs GPS Time difference after the offline
384 correction. The shorter the correction time window, the better. However,
385 with the medium length time window, we still get time residuals lower than
386 3 ns over the whole data-taking period, which is well below the requirements
387 of HK. With the longest correction time window, jumps of a few tens of
388 nanoseconds are introduced in the time residuals. This explains the overall
389 higher ASD: the stability of the signal is limited by those jumps. **Later,**
390 **if necessary, add plot with fitted time differences.** The time scale
391 of the variations in the data to fit is too small compared to the 240,000 s
392 time window. In consequence, the fitted tendency from one piece to another
393 is very different, and the fitted piece-wise polynomial is not continuous. It
394 is also interesting, as a cross-check, to have a look at the fluctuations in
395 the time difference between the Rubidium clock and the UTC(OP) after
396 correction. This is summarized in the first line of Table 2 that gives the
397 standard deviation of the time series after correction. The deviations with
398 the two shorter correction time windows are indeed very small (below 2 ns)
399 confirming that this method can be used for synchronization to UTC.

400 With the offline version of the corrections, we thus obtain a very good
401 synchronization to GPS Time at the level of a few nanoseconds with the
402 10560 s time window. However, this version of the correction cannot be
403 applied in real time. In the following, we show the results for the online
404 version of the correction that can be applied in real time to correct the time
405 stamps of events in physics experiments.

406 3.2. Online correction

407 Figure 13 shows the Allan Standard Deviation of the uncorrected (blue)
408 and online corrected (other colors) Rubidium - UTC(OP) times series. The

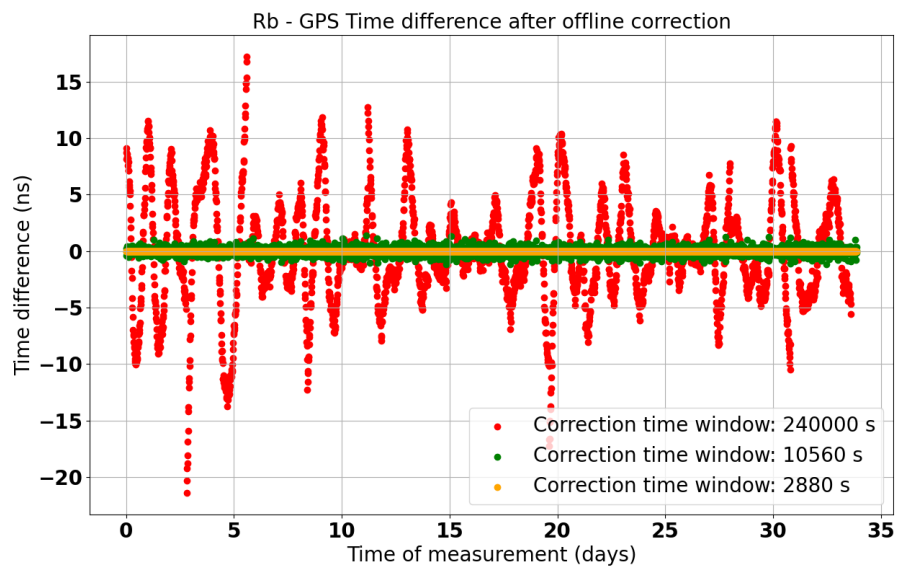


Figure 12: Time difference between the Rubidium clock and GPS Time after the offline correction. Three different correction time windows have been tested: 2800 s (orange), 10560 s (green) and 240,000 s (red). These residuals can be compared to the residuals before correction that were shown in Figure 10.

409 same three time windows intervals as in the offline correction scenario are con-
410 sidered. The top panel shows the results using quadratic fits of the Septentrio
411 data and the bottom panel shows the results with linear fits. For the shortest
412 and medium correction time windows, the linear fits lead to better perfor-
413 mance with a lower OASD at low averaging times. At 1000 s, the OASD
414 with the shortest (medium) correction time window is reduced by a factor 2
415 to 3 (resp. ~ 1.5).

416 This behavior can be understood by looking at the number of degrees of
417 freedom (number of data points - number of free parameters) in our fits. For
418 the shortest time windows, the number of degrees of freedom is relatively
419 low (0 and 8) in case of quadratic fits so we risk over-fitting to the past
420 data in order to correct the present data. This number of degrees of freedom
421 is less relevant in the offline correction as the fit is performed on the same
422 data as the correction (the over-fitting is not a problem here). Lowering the
423 number of free parameters is one way of increasing the degrees of freedom
424 hence allowing the fit to better generalize to the present data. Another way
425 to increase the number of degrees of freedom is to increase the number of
426 data points in the fit. For the longest time window, there are 247 degrees
427 of freedom in the quadratic fit so we lower the risk of over-fitting. On the
428 contrary, in that case, quadratic fits lead to a slightly better correction of
429 the random walk that limits the stability only up to $\tau \approx 3 \times 10^4$ s whereas
430 with linear fits, it limits the stability up to $\approx \times 10^5$ s. Note that, especillay
431 for the shortest correction time window we see a clear degradation of the
432 stability for averaging times lower than the correction window's length. This
433 is a known effect from linear servo loop theories and periodic perturbations
434 of oscillators [32] and it could be attenuated by scaling down the correction:
435 instead of subtracting the result of the fit, we could subtract only a fraction
436 of it.

437 **Removed the Rb-GPS OASD because not sure it is necessary.**
438 **Could be added in annex.**

439 Regarding the stability of the corrected Rubidium clock, using linear fits,
440 the conclusions are the same as for the offline correction. The lowest Allan
441 Standard Deviation, for all averaging times, is achieved with the medium
442 width correction time window. With the shortest time window, the short
443 term stability is degraded, and the long term stability is also degraded (com-
444 pared to the other corrected scenarios) with the longest correction time win-
445 dow.

446 If the correction time window is too wide, we cannot correct as well the

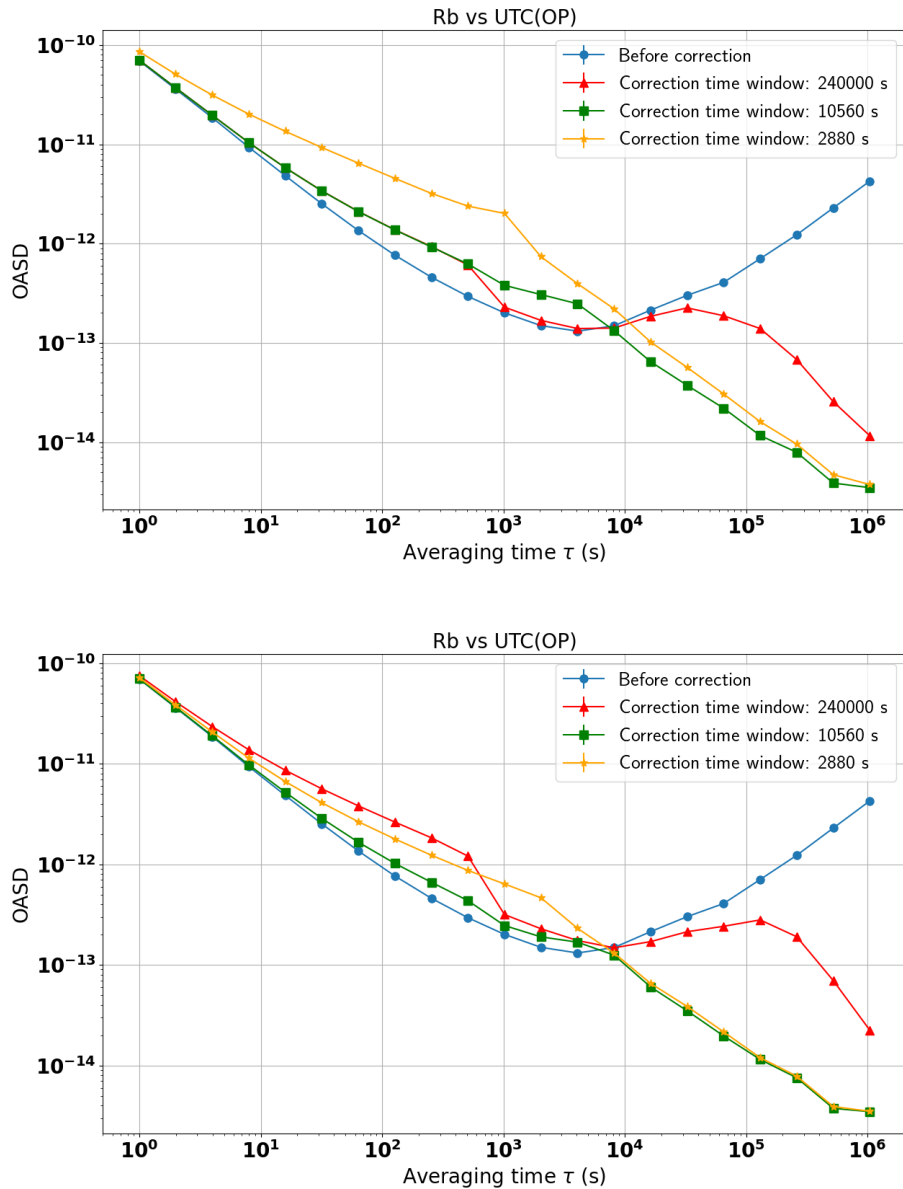


Figure 13: Overlapping Allan Standard Deviation of the Rb/PHM frequency ratios series after the deterministic drift correction (in blue) and after the online correction with a correction time window of 2880 s (orange), 10560 s (green) and 240,000 s (red). The data were fitted with quadratic (top) or linear (bottom) functions of time. A better stability, similar to the offline correction, can be obtained using linear fits.

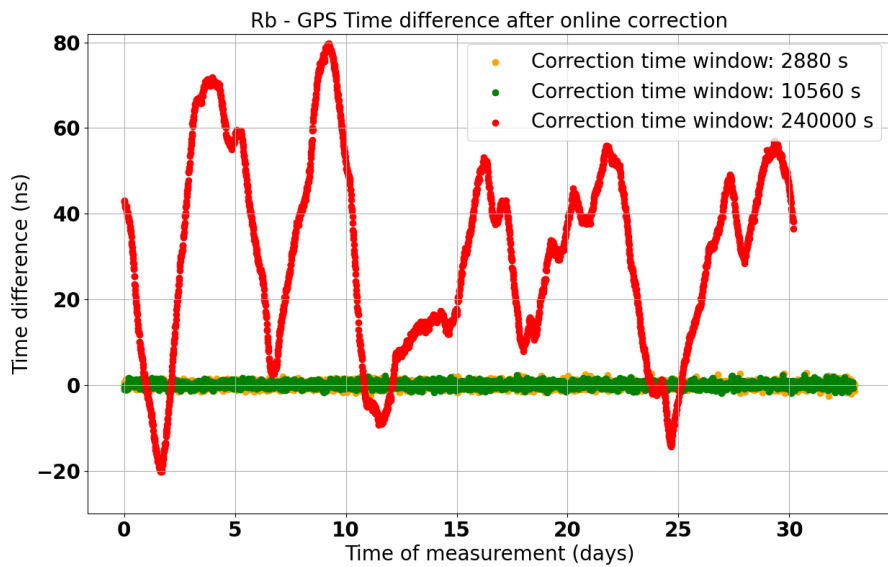
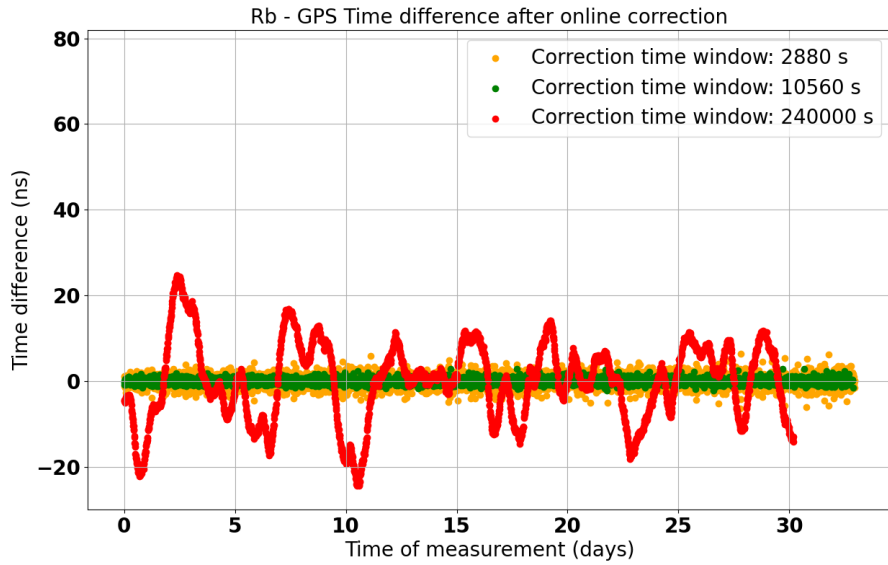


Figure 14: Time difference between the Rubidium clock and GPS Time after the online correction. Each point is corrected using a quadratic (top) or linear (bottom) fit of the 2800 s (orange) or 10560 s (green) or 240,000 s (red) of data points prior to this point. Using linear fits leads to smaller residuals for the shortest time window and bigger ones for the longest time window.

correction time window	2880 s	10560 s	240000 s
offline correction	1.87 ns	1.79 ns	5.13 ns
online correction (quadratic fits)	2.01 ns	1.83 ns	9.35 ns
online correction (linear fits)	1.84 ns	1.81 ns	22.66 ns

Table 2: Standard deviation of the time difference between the Rubidium clock PPS signal and the UTC(OP) after correction.

447 frequency random walk of the free-running Rubidium: the risk is that the
448 Rubidium time signal locally drifts too far away from the GPS Time. This
449 can be observed in the corrected Rubidium against GPS Time in Figure 14
450 where the maximum difference reaches ~ 80 ns (or ~ 25 ns with quadratic
451 fits) with the 240,000 s correction time window. With the 10560 s correc-
452 tion time window, the differences stay in the ± 5 ns range. The standard
453 deviation of the time difference with the UTC(OP) is also chosen in Table
454 2 for both online corrections. Once again, one can see the reduction of the
455 white noise when using linear instead of quadratic fits. Before correction,
456 as the reader saw in Figure 10, the free-running Rubidium clock can drift
457 away from the GPS Time by around 100 ns in less than 3 days which means
458 that HK's requirement for the synchronization with UTC is not met. After
459 online correction with the longest time window tested, the corrected Rubid-
460 ium time stamps drift by around 60 ns in a few days because of remaining
461 random walk noise. Even though during the 35 days data-taking period the
462 time residuals with respect to GPS Time does not exceed 100 ns, it is not
463 possible to safely claim that the Rubidium clock drift will not exceed HK's
464 requirement of 100 ns if we use the 240,000 s correction time window. With
465 shorter time windows, this drift seems to be dominated by white noise and
466 is thus contained in a range of a few nanoseconds.

467 4. Discussion

468 As advertised before, the advantage of the so-called online correction is
469 that it could be performed in real-time. This is an important feature for
470 applications that necessitate a real-time synchronization with UTC or with
471 another site (like the future HK or DUNE experiments). If a reference clock
472 signal is generated with an atomic clock (like the Rubidium clock used here)
473 and sent to a data acquisition system to be propagated to detectors and pro-
474 vide time stamps, one could continuously compare this signal to GPS Time

475 using a Septentrio receiver. The correction coefficients a , b and c calculated
 476 from the Septentrio data would need to be sent to the data acquisition system
 477 so that it could correct the time stamps in real-time.

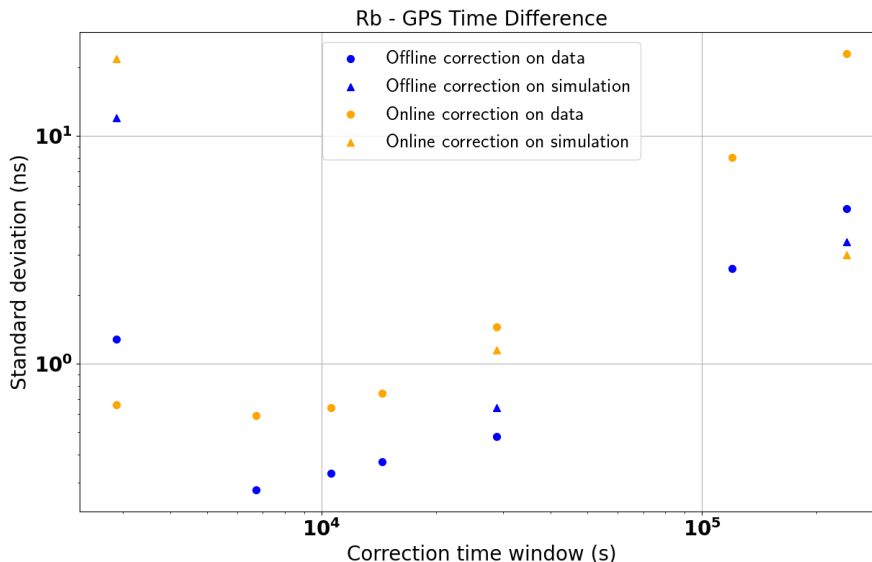


Figure 15: Standard deviation of the residuals distributions between the Rb and the GPS Time after the offline (blue) or online (orange) correction as a function of the correction time window. Quadratic fits of the Septentrio data are used for the offline correction whereas linear fits are used for the online correction. The performance on simulated data is also shown for the three usual correction time windows.

478 Figure 15 shows the standard deviation of the Rb vs GPS Time differ-
 479 ence after correction as a function of the correction time window's width. The
 480 performance of the offline and online corrections on experimental data (col-
 481 ored dots) are compared to the performance we had obtained on simulated
 482 data (colored triangles) with a correction time window of 2880 s, 28800 s
 483 and 240000 s. Note that these simulated data were only taking into account
 484 phase white noise, frequency white noise and frequency random walk com-
 485 ponents. In particular, the measured data also contains a linear frequency
 486 drifts and this main difference alone could explain the difference of perfor-
 487 mances between data and simulation. Also, no additional uncertainties were
 488 added to take into account other types of noise (e.g: flicker noise) or experi-
 489 mental conditions (e.g: imperfect calibrations, imperfect PHM time signal).

490 For both corrections, very similar performance of synchronization with GPS
491 Time are obtained for correction time windows below 30,000 s so there is no
492 need to have much shorter windows. This result is consistent with the fact
493 that, as seen in Figure 2, the stability of the Rubidium signal becomes worse
494 than that of the GPS around 10^4 s. The offline correction seems to provide
495 a slightly better synchronization to GPS Time (down to ~ 0.3 ns **update**)
496 but the precision achievable with the online correction is already more than
497 satisfying (better than 5 ns for correction time windows below 100,000 s) for
498 synchronization between several experimental sites. Indeed, the needed level
499 of synchronization is usually of the order of 100 ns for those applications.

500 5. Conclusions

501 In this paper, we presented a simple way to use time comparisons to
502 GPS Time to synchronize the time stamps, generated using a free-running
503 Rubidium clock, close to UTC while preserving its short term stability and
504 correcting the long term frequency random walk and deterministic drift. This
505 method has the advantage of using relatively cheap instruments and to be ap-
506 plicable online for a real-time synchronization as well as to be robust against
507 GPS signal reception failures. The online method could be applied for the
508 real-time synchronization between several experimental sites in long-baseline
509 neutrino physics experiments.

510 This method consists in fitting the GPS Time vs Rubidium measured by a
511 GNSS receiver with a piece-wise polynomial function of time and in subtract-
512 ing the result to the generated time stamps. The method was first designed
513 and validated with simulated signals before assessing its performance on real
514 data. We evaluated the performance of this correction by quantifying the sta-
515 bility of the clock signal before and after the correction using the Overlapping
516 Allan Standard Deviation. We showed that the optimal length of the time
517 window for the fit of the GPS Time vs Rubidium seats around 10,000 sec-
518 onds, corresponding to ~ 10 data points from the receiver. This time window
519 allowed to maintain the best possible short term stability while correcting ef-
520 ficiently the frequency random walk. After correction with this time window,
521 the difference to GPS Time stays within a window of ± 5 ns for both offline
522 and online corrections during the whole period of ~ 35 days of measurement.
523 This performance largely meets the usual requirements for long-baseline neu-
524 trino physics experiments, like Hyper-Kamiokande and DUNE. Note that we
525 do not expect the performance of the correction to be heavily degraded by

526 isolated missing or outlier measurements from the receiver. However, this
527 correction requires a constant monitoring of the Rubidium time signal with
528 a GNSS receiver (or other reference that can be linked to UTC). One should
529 thus make sure that such a reference is available in the long term and that
530 there is no possibility to loose it for long periods (e.g.: several hours).

531 **Fundings:** This research was funded by IN2P3/CNRS, the French "Agence
532 nationale pour la recherche" under grant number ANR-21-CE31-0008, the
533 "IdEx Sorbonne Université" and the 2019 "Sorbonne Université Émergences:
534 MULTIPLY" grant.

535 The White Rabbit network and the access of associated optical fibers to
536 the Pierre and Marie Curie campus: T-REFIMEVE, FIRST TF and LNE:
537 "Agence Nationale de la Recherche" (ANR-21-ESRE-0029 / ESR/Equipex T-
538 REFIMEVE, ANR-10-LABX48-01 / Labex First-TF); Laboratoire National
539 d'Essai (LNE), project TORTUE.

540 References

- 541 [1] M. Guler et al., *OPERA: An appearance experiment to search for ν/μ
542 $\leftrightarrow \nu/\tau$ oscillations in the CNGS beam*, Experimental proposal,
543 CERN-SPSC-2000-028.
- 544 [2] K. Abe et al., T2K Collaboration, *The T2K Experiment*, *Nucl. In-*
545 *strum. Meth. A* **659** (2011), 106-135, doi:10.1016/j.nima.2011.06.067,
546 arXiv:1106.1238.
- 547 [3] D. S. Ayres et al., *The NOvA Technical Design Report*, (2007),
548 doi:10.2172/935497.
- 549 [4] K. Abe et al., *Hyper-Kamiokande Proto-Collaboration, Hyper-*
550 *Kamiokande Design Report*, (2018), arXiv:1805.04163.
- 551 [5] B. Abi et al., *Deep Underground Neutrino Experiment (DUNE), Far*
552 *Detector Technical Design Report, Volume I: Introduction to DUNE*,
553 (2020), arXiv:2002.02967.
- 554 [6] D. Cussans et al., *Timing and synchronization of the DUNE neutrino*
555 *detector*, *Nuclear Instruments and Methods in Physics Research, A* **958**
556 (2020), doi:10.1016/j.nima.2019.04.097.

- 557 [7] P. Mészáros, D.B. Fox, C. Hanna et al., *Multi-messenger astrophysics*,
558 *Nat. Rev. Phys.* **1** (2019) 585–599, [https://doi.org/10.1038/s42254-019-](https://doi.org/10.1038/s42254-019-0101-z)
559 0101-z.
- 560 [8] The Supernova Early Warning System web page, <https://snews2.org/>.
- 561 [9] K. Abe et al., T2K collaboration, *Upper bound on neutrino*
562 *mass based on T2K neutrino timing measurements*, *Physical Re-*
563 *view D* **93** (2016) 1, 012006, doi: 10.1103/PhysRevD.93.012006,
564 <https://arxiv.org/abs/1502.06605>.
- 565 [10] Y. Fukuda et al., Super-Kamiokande collaboration, *The Super-*
566 *Kamiokande detector*, *Nucl.Instrum.Meth.A* **501** (2003) 418,
567 [https://doi.org/10.1016/S0168-9002\(03\)00425-X](https://doi.org/10.1016/S0168-9002(03)00425-X).
- 568 [11] L. Mellet, M. Guigue, B. Popov, S. Russo, V. Voisin, on behalf of the
569 Hyper-Kamiokande Collaboration, *Development of a Clock Generation*
570 *and Time Distribution System for Hyper-Kamiokande*, *Phys. Sci. Forum*
571 **8** (2023) 72, <https://doi.org/10.3390/psf2023008072>.
- 572 [12] M. Lombardi, *Fundamentals of Time and Frequency*, *The Mechatronics*
573 *Handbook*, CRC Press: Boca Raton, FL, USA (2002), ISBN 978-0-8493-
574 6358-0.
- 575 [13] Giulia Brunetti, *Neutrino velocity measurement with the OPERA exper-*
576 *iment in the CNGS beam*, Université Claude Bernard - Lyon I; Univer-
577 sità degli studi (Bologne, Italie), 2011. English. ⟨NNT : 2011LYO10088⟩.
578 ⟨tel-00843100⟩
- 579 [14] M.A. Weiss, G. Petit, Z. Jiang, *A comparison of GPS common-view*
580 *time transfer to all-in-view*, In Proceedings of the *IEEE International*
581 *Frequency Control Symposium and Exposition*, 2005.
- 582 [15] The National Institute of Information and Communications Technology
583 (NICT), Japan. <https://www.nict.go.jp/en/>
- 584 [16] <https://www.bipm.org/en/time-ftp/circular-t>
- 585 [17] D.A. Howe, D.W. Allan, J.A. Barnes, *Properties of signal sources and*
586 *measurement methods*, In Proceedings of the Thirty Fifth Annual Fre-
587 quency Control Symposium, Philadelphia, USA, 27-29 May 1981.

- 588 [18] J. Serrano et al., *The White Rabbit project* (2013),
589 <https://cds.cern.ch/record/1743073>.
- 590 [19] G. Daniluk, *White Rabbit calibration procedure (version 1.1)*
591 (2015), [https://white-rabbit.web.cern.ch/documents/WR_Calibration-](https://white-rabbit.web.cern.ch/documents/WR_Calibration-v1.1-20151109.pdf)
592 [v1.1-20151109.pdf](https://white-rabbit.web.cern.ch/documents/WR_Calibration-v1.1-20151109.pdf)
- 593 [20] E. Cantin et al., *REFIMEVE Fiber Network for Time and Frequency*
594 *Dissemination and Applications*, 2023 Joint Conference of the Euro-
595 pean Frequency and Time Forum and IEEE International Frequency
596 Control Symposium (EFTF/IFCS), Toyama, Japan, 2023, pp. 1-4, doi:
597 10.1109/EFTF/IFCS57587.2023.10272084.
- 598 [21] C. B. Lim et al., *Extension of REFIMEVE with a White Rab-*
599 *bit Network*, 2023 Joint Conference of the European Frequency
600 and Time Forum and IEEE International Frequency Control
601 Symposium (EFTF/IFCS), Toyama, Japan, 2023, pp. 1-4, doi:
602 10.1109/EFTF/IFCS57587.2023.10272069.
- 603 [22] G. D. Rovera et al., *UTC(OP) based on LNE-SYRTE atomic fountain*
604 *primary frequency standards*, *Metrologia* **53** (2016) S81.
- 605 [23] <https://webapp.csr-scrs.nrcan-rncan.gc.ca/geod/tools-outils/ppp.php>
- 606 [24] P. Defraigne, G. Petit, *CGGTTS-Version 2E: an extended standard*
607 *for GPS Time Transfer*, *Metrologia* **52** (2015), IOP Publishing, doi:
608 10.1088/0026-1394/52/6/G1.
- 609 [25] J. Plumb et al., *Absolute calibration of a geodetic time transfer system,*
610 *Ultrasonics, Ferroelectrics and Frequency Control, IEEE Transactions*
611 **52** (2005) 1904-1911, doi: 10.1109/TUFFC.2005.1561658.
- 612 [26] G. D. Rovera et al., *Link calibration against receiver calibration time*
613 *transfer uncertainty when using the Global Positioning System*, *Metrolo-*
614 *gia* **51.5** 476490 (2014).
- 615 [27] Lucile Mellet, *From T2K to Hyper-Kamiokande : neutrino oscillation*
616 *analysis and preparation of the time synchronization system*, PhD thesis,
617 Sorbonne University (2023), ⟨NNT : 2023SORUS297⟩ ⟨tel-04284182⟩.

- 618 [28] J. A. Barnes et al., *Characterization of Frequency Stability*, in *IEEE*
619 *Transactions on Instrumentation and Measurement*, vol. IM-20, no. 2,
620 pp. 105-120, May 1971, doi: 10.1109/TIM.1971.5570702.
- 621 [29] T. J. Witt, *Using the Allan variance and power spectral density to*
622 *characterize DC nanovoltmeters*, in *IEEE Transactions on Instrumen-*
623 *tation and Measurement*, vol. 50, no. 2, pp. 445-448, April 2001, doi:
624 10.1109/19.918162.
- 625 [30] D. W. Allan, *Statistics of atomic frequency standards*, in *Proceed-*
626 *ings of the IEEE*, vol. 54, no. 2, pp. 221-230, Feb. 1966, doi:
627 10.1109/PROC.1966.4634.
- 628 [31] W. J. Riley, *Handbook of frequency stability analysis*, *NIST* Special pub-
629 lication 1065, July 2008.
- 630 [32] G. Santarelli, C. Audoin, A. Makdissi, P. Laurent, G. J. Dick, et A. Cla-
631 iron, *Frequency stability degradation of an oscillator slaved to a periodi-*
632 *cally interrogated atomic resonator*, *IEEE Transactions on Ultrasonics,*
633 *Ferroelectrics, and Frequency Control* **45** n 4 (juill. 1998) p. 887-894,
634 doi: 10.1109/58.710548.